geoconvention
Virtual Event
September 13 - 15
2021

Surface wave full waveform inversion with the data collected from a trench deployed Distributed Acoustic Sensing survey

Luping Qu, University of Calgary, Wenyong Pan, Key Laboratory of Petroleum Resource Research, Institute of Geology and Geophysics, Chinese Academy of Sciences, Kristopher A. Innanen, Jan Dettmer, University of Calgary, Marie Macquet, Donald Lawton, University of Calgary and CMC

Summary

Distributed acoustic sensing (DAS) is a rapidly developing technology for seismic monitoring, conferring advantages such as dense spatial sampling, unobtrusiveness, and relatively inexpensive installation. At the Containment and Monitoring Institute Field Research Station (CaMI.FRS) in Newell County, Alberta, Canada, a range of seismic field experiments with DAS have been carried out to validate it as a tool for monitoring of carbon capture and storage. Horizontal lengths of the DAS cable are natural sensors of surface wave arrivals from seismic sources, and the opportunity presents itself to investigate the use of these arrivals to characterize the near surface. DAS-recorded surface waves are spatially un-aliased, and relative to most geophones have a strong low frequency component. A full waveform inversion (FWI) workflow was applied to image the near-surface S-wave velocity structure using the DAS-recorded surface waves. Compared to traditional surface-wave analysis, we show that FWI intrinsically incorporates fundamental and high-order modes and provides high-resolution S-wave velocity models that resolve lateral variations. The low frequencies in the DAS data are particularly helpful to overcome cycle skipping. The inversion result represents a detailed characterization of the near-surface shear-wave velocity profile.

Method

In 2018, a large multi-offset, multi-azimuth VSP data set was acquired at the CaMI.FRS by University of Calgary researchers and several industrial partners (Hall et al., 2019). Because the DAS fiber in the geophysics well is part of a 5km loop which includes a roughly 1km long horizontal trenched section, and because numerous source points lay along the trench, a subset of the 2018 DAS data was a 1-150Hz 2D surface line, which was used in this study (Figure 1a). The DAS response (strain rate) can be related to particle velocities by

$$\dot{\epsilon_{xx}} = \frac{1}{L}\left[v_x\left(z+\frac{L}{2}\right) - v_x\left(z-\frac{L}{2}\right)\right],$$

Where "." Denotes time derivatives, v_x is the tangential particle velocity, L is gauge length (10 m in this case), and z is the center of the gauge. Different approaches can be used to convert DAS strain rate to particle velocity (or displacement). Converted DAS data can closely match geophone measurements in both amplitude and phase (Daley et al., 2016). In particular, Daley showed that the strain rate signal can be converted to equivalent velocity units via scaling by apparent velocity. Considering a propagating harmonic plane wave, its displacement and particle velocity fields in the x direction are

$$u_x = U\mathbf{exp}\left[-i\omega\left(t-\frac{x}{c}\right)\right],$$

$$v_x = \frac{du_x}{dt} = U(-i\omega)\mathbf{exp}\left[-i\omega\left(t-\frac{x}{c}\right)\right],$$

where U is the amplitude of the plane wave, c is apparent velocity, i is the imaginary unit, and ω is angular frequency. Therefore, strain is given by (Benioff, 1932)

$$\epsilon_{xx} = \frac{\partial u_x}{\partial x} = \frac{u_x dt}{dx} = \pm\frac{u_x}{c},$$

where $\pm$ is the direction of wave propagation. Therefore, the scaling from strain to velocity is apparent velocity, and the DAS signal can be converted to geophone-signal units. However, limitations exist due to noise in field data which may be amplified by this conversion.

Compared with the traditional geophone data, the DAS surface-wave data are more coherent and do not suffer from spatial aliasing. The fundamental and high-order surface-waves can be clearly identified. Frequencies below 10 Hz are important for overcoming the cycle-skipping problems in FWI and these frequencies are poorly recorded by the 10 Hz geophones.

Application to surface-waves at CaMI.FRS

In a typical FWI formulation, model parameters are iteratively updated by minimizing the direct waveform-difference (WD) formulated as a L-2 norm, e.g.,

$\Phi(\mathbf{m}) = \frac{1}{2}\sum_{i=1}^{N_s}\sum_{j=1}^{N_t}\left[\mathbf{d}_{\text{syn}}(\mathbf{x}_r^i, t_j; \mathbf{m}) - \mathbf{d}_{\text{obs}}(\mathbf{x}_r^i, t_j)\right]^2$,

where $\mathbf{m}$ is the model vector, $\mathbf{d}_{\text{syn}}$ and $\mathbf{d}_{\text{obs}}$are synthetic and observed seismic data, respectively, at $\mathbf{x}_r^i$ reciever locations and t_j time samples. Sensitivity kernel (or gradient) of V_S can be calculated by cross-correlating the forward and adjoint wavefields based on the adjoint-state method

$K_{V_S} = -2\rho V_S^2\left[\partial_j u_i^*\left(\partial_i u_j + \partial_j u_i\right) - 2\,\partial_i u_i^*\,\partial_k u_k\right]$,

where u^* are adjoint wavefields. We apply L-BFGS optimization and line search methods to calculate search directions and step lengths (Nocedal & Wright, 2006) to refine the model iteratively. The WD misfit function is applied to surface-wave data recorded on surface-trenched fibre at CaMI.FRS to obtain a near-surface V_S model. A spectral-element method is applied for forward modeling. The inversion is carried out with the open-source package SeisElastic2D (Pan et al., 2020). An initial 1D V_P velocity model is created from well-log data with Gaussian smoothing (Figure 1b). The 1D initial density (ρ model) is created by applying Gardner's rule to the V_P model, followed by Gaussian smoothing. Finally, the 1D V_S model is generated by the traditional SWD method for 0- to 100-m depth. The 2D initial V_S model was obtained by extending the result of SWD. The initial V_S model below 100 m is created with $V_P/V_S = 2.2$.

We first carry out isotropic elastic inversion to invert for V_S model. Both observed and synthetic data are normalized trace-by-trace, which removes the attenuation effects on seismic amplitudes. The source-time function for forward modeling is a Klauder wavelet with a linear frequency modulated sweep from 1 to 150 Hz. A three-stage strategy is applied for the inversion: In stage I, the fundamental mode of surface-waves is extracted from the shot gathers for inversion. In stage II, high-order modes are extracted for inversion. In stage III, shot gathers with both fundamental and high-order surface-wave modes are used. At each stage, a multi-scale strategy is employed by first filtering to a frequency band of [4, 16] Hz and subsequently to [4, 20] Hz. The source-time function is filtered correspondingly.

Figure 2 shows the comparison between initial and inverted V_S models. The inverted V_S model exhibits a significant velocity contrast at the depth of ~25 m, which corresponds to the boundary of overburden with the Dinosaur Park formation. At depths of ~25 to 100 m, lateral variability is evident in the V_S results. These depths correspond to the Dinosaur Park formation. Fundamental-mode surface-waves mainly contributed to constrain the shallow V_S model from 0 to 50 m. The high-order modes and low-frequencies are important to recover the low-wavenumber V_S structure

at greater depths. After incorporating the higher-order modes, the deeper V_S structures at the depths from 50 m to 200 m is better resolved. Compared to the synthetic data calculated using the initial V_S model, the synthetic data obtained from the inverted V_S model match more closely with the observed data.

Conclusions

We have applied FWI to DAS-recorded surface-waves at the CaMI.FRS monitoring site in Alberta, Canada. Compared to 10-Hz geophone data, DAS data has the advantages of dense spatial sampling and containing lower-frequencies. These advantages help overcome the cycle skipping problem of FWI. Finally, FWI produces high-resolution S-wave velocity model with lateral variations using both fundamental and high-order surface-waves recorded by DAS. The inverted near-surface S-wave velocity structures can provide valuable information for CO_2 sequestration and monitoring.

Acknowledgements

This work was funded by the industrial sponsors of the Consortium for Research in Elastic Wave Exploration Seismology (CREWES), and by the NSERC grants CRDPJ 461179-13 and CRDPJ 543578-19. We gratefully acknowledge continued support from CREWES sponsors. Wenyong Pan is supported by National Natural Science Foundation of China (Grant No. E1115401) and IGGCAS Research Start-up Funds (Grant No. E0515402). Luping Qu is supported by the Earl D. and Reba C. Griffin Memorial Scholarship through the SEG Foundation. The authors also acknowledge CMC for providing access to the field site which is supported by the University of Calgary's Canada First Research Excellence Fund program: the Global Research Initiative in Sustainable Low-Carbon Unconventional Resources.

References

Benioff, H., 1932, A new vertical seismograph: Bulletin of the Seismological Society of America, 22, 155–169.
Daley, T. M., D. E. Miller, K. Dodds, P. Cook, and B. M. Freifeld, 2016, Field testing of modular borehole monitoring with simultaneous distributed acoustic sensing and geophone vertical seismic profiles at Citronelle, Alabama: Geophysical Prospecting, 64, 1318–1334.
Hall, K., M. Bertram, K. Bertram, K. A. Innanen, and D. C. Lawton, 2019, Simultaneous accelerometer and optical fibre multi-azimuth walk-away VSP experiment: Newell County, Alberta, Canada: SEG Expanded Abstracts, 5340–5344.
Nocedal, J. and S. J. Wright, 2006, Numerical optimization: Springer.
Pan, W., K. A. Innanen, and Y. Wang, 2020, SeisElastic2D: An open-source package for multiparameter full-waveform inversion in isotropic-, anisotropic- and visco-elastic media: Computers & Geosciences, 145, 104586.

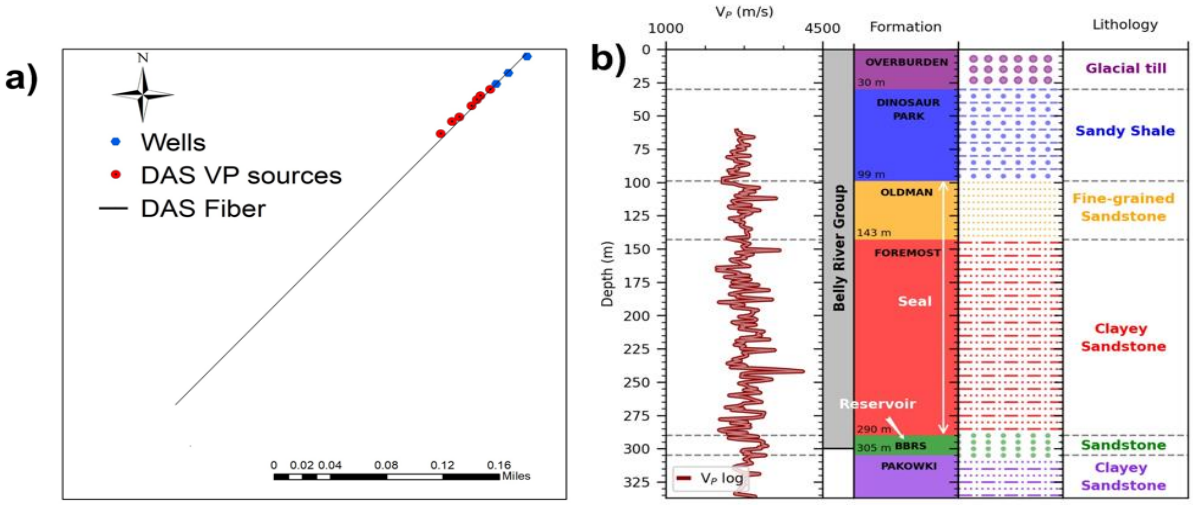

Figure 1: (a) Geometry of collected DAS data. The red dots are the source points, the black line is the fiber, the blue dots are three wells while the middle one is the injection well, (b) The P-wave velocity VP well log of the injection well (red line), the geological formations and lithology distributions at CaMI.FRS.

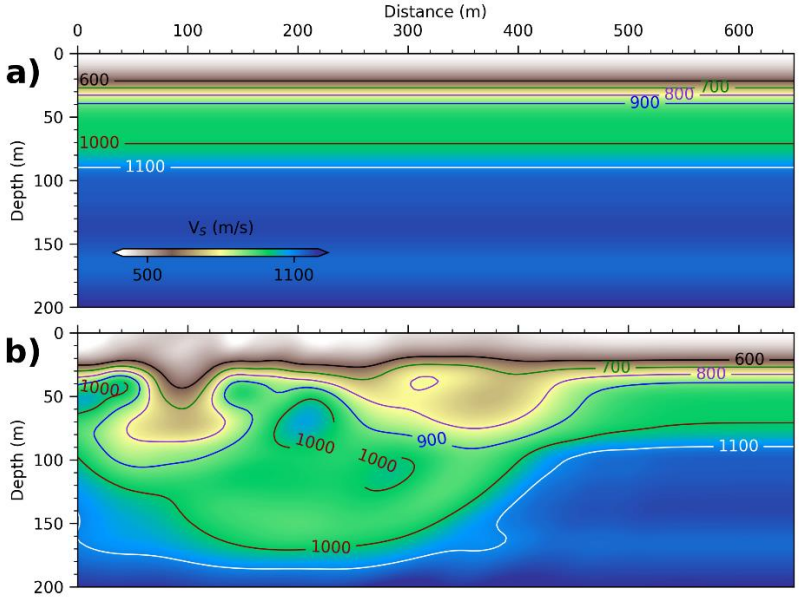

Figure 4: (a) Inverted Vs model; (b) Inverted Qs model.